The International Archives of the Photogrammetry, Remote Sensing and Spatial Information Sciences, Volume XLVIII-2/W9-2025
ISPRS Intl. Workshop "Photogrammetric and computer vision techniques for environmental and infraStructure monitoring, Biometrics and Biomedicine"
PSBB25 , 9–11 June 2025, Moscow, Russia

Data augmentation using Fast and Adaptive Bidimensional Empirical Mode Decomposition for pulmonary tuberculosis diagnosis in chest X-rays

Yuliya D. Senotova [1], Yakov A. Pchelintsev [2], Andrey S. Krylov [3]

[1] Faculty of Computational Mathematics and Cybernetics, Lomonosov Moscow State University, Moscow, Russia - yulsenva@gmail.com
[2] Faculty of Computational Mathematics and Cybernetics, Lomonosov Moscow State University, Moscow, Russia - pchelintsev@cs.msu.ru
[3] Faculty of Computational Mathematics and Cybernetics, Lomonosov Moscow State University, Moscow, Russia – kryl@cs.msu.ru

Keywords: chest X-ray, medical images, pulmonary tuberculosis diagnosis, data augmentation, deep learning, Fast and Adaptive Bidimensional Empirical Mode Decomposition.

Abstract

Automation in medical diagnostics based on machine learning algorithms relies heavily on the quality and volume of training data. For pulmonary tuberculosis diagnosis in chest X-rays image quality varies due to differences in equipment and acquisition conditions, and the availability of high-quality data is limited due to legal constraints and the smaller size of public datasets compared to those for some other lung diseases. Additionally, concerns regarding cross-dataset compatibility and discrepancies between training and target data distributions further complicate the analysis. To mitigate these issues, we propose a data augmentation technique utilizing the Fast and Adaptive Bidimensional Empirical Mode Decomposition (FABEMD) algorithm. Experiments have demonstrated its effectiveness for pulmonary tuberculosis diagnosis in chest X-rays.

1. Manuscript

Tuberculosis is an infection with high mortality causing more than a million deaths each year. Despite the fact that research and medical efforts have succeeded in reducing mortality from tuberculosis, the incidence rate has only increased in recent years (World Health Organization, 2024). Pulmonary tuberculosis (TB) is the most prevalent form of TB. Chest X-ray (CXR) review is an effective tool for screening lung diseases, including TB, due to its non-invasiveness and availability, but it requires trained radiologists to interpret the images.

For pulmonary tuberculosis (TB) diagnosis in chest X-rays the quality of images is highly dependent on the equipment, its settings and other acquisition conditions, collecting a large volume of images is not easy due to limited number of patients and legal reasons, and publicly available chest X-ray datasets for pulmonary tuberculosis diagnosis (Oloko-Oba and Viriri, 2022, Zeyu et al., 2022, Singh et al., 2022, Santosh et al., 2022) are smaller than those for some other pulmonary diseases. Besides, cross-dataset compatibility degree and difference of training and real-world data distributions for chest X-ray analysis are of big concern (Pooch et al., 2020, Xue et al., 2023, Pchelintsev et al., 2023).

As for data standardization preprocessing techniques in CXR analysis, the most common method is local contrast enhancement by local histogram equalization (CLAHE) (Pizer et al., 1987), but some other examples are: automatic gamma correction, balance contrast enhancement technique (Rahman et al., 2021). More complex medical image enhancement methods also exist (PLIP unsharp masking (Zhao and Zhou, 2016), multiscale Retinex (Setty et al., 2013), TV-homomorphic (Rui and Guoyu, 2017), G-CLAHE (Nia and Shih, 2024), but they are not commonly used as a deep learning preprocessing step.

To cope with the lack of data and increase coverage of data distribution in machine learning, augmentation techniques are used. Typical methods for image data include random crops, affine transformations, brightness, contrast and color adjustment, label fusion, adding noise. In this paper we present a method of chest X-ray data augmentation for pulmonary tuberculosis diagnosis using the Fast and Adaptive Bidimensional Empirical Mode Decomposition (FABEMD) algorithm (Bhuiyan et al., 2008a, Bhuiyan et al., 2008b).

2. Empirical Mode Decomposition Algorithms Overview

2.1 EMD Overview

Empirical Mode Decomposition (EMD) (Huang et al., 1998) is an iterative method of representing input signal as a sum of intrinsic mode functions (IMFs) and a residue R:

$$\mathrm{I} = \sum_{k} \mathrm{IMF}_k + \mathrm{R},$$

where k is the intrinsic mode number. An IMF must satisfy two conditions: (1) the number of extrema and the number of zero crossings must either equal or differ at most by one; (2) at any point, the mean value of the envelope defined by the local maxima and the envelope defined by the local minima is zero.

The idea of EMD at the k-th iteration is to find local maxima and minima of the function

$$\mathrm{J} = \mathrm{I} - \sum_{i=1}^{k-1} \mathrm{IMF}_i$$

and construct its upper and lower envelopes using spline interpolation. The average of the envelopes E_m is calculated, and

the quotient $\mathrm{J} - \mathrm{E}_m$ is considered to be the new IMF_k (or can be refined further by the same procedure) and $\mathrm{J} - \mathrm{IMF}_k$ is treated as the signal for the next iteration. The stopping criteria may include the monotony or the standard deviation of the residue and the maximum number of IMFs.

The first IMFs contain high frequency information, and with the growth of the IMF number more coarse structures are stored in the corresponding IMF. The last IMF with information of the lowest frequencies is called residue. An example of the EMD result of a 1D signal is shown in Fig. 1.

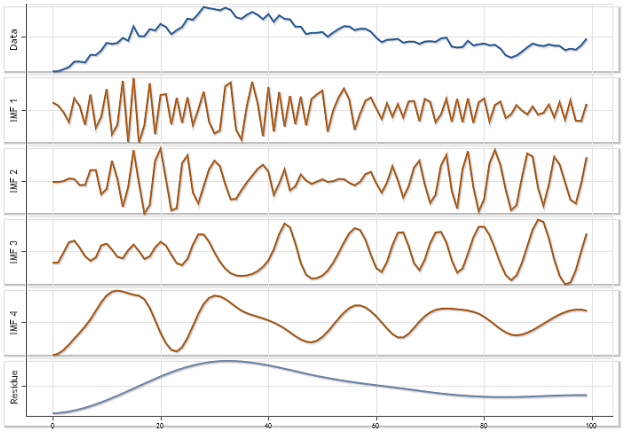

Figure 1. An example of a function (top), its IMFs (brown) and the residue (bottom) obtained by EMD (Victor, 2012)

EMD has some limitations, including the computational complexity, the unpredictability of the IMFs obtained due to noise contamination, the unpredictability of the IMFs number for a given signal, the boundary effects caused by the spline interpolation (Sweeney-Reed et al., 2018).

2.2 FABEMD overview

An alternative to EMD for two-dimensional functions, in particular images, called bidimensional EMD (BEMD) was presented in (Nunes et al., 2003). Although IMFs of BEMD may not satisfy all EMD conditions presented in the original paper, BEMD is just as much empirical and replicates the spatial feature extraction procedure of EMD. However, for multiple dimensions computational complexity is greatly increasing, thus another approach called Fast and Adaptive Bidimensional Empirical Mode Decomposition (FABEMD) was proposed in (Bhuiyan et al., 2008a, Bhuiyan et al., 2008b). Despite its name, it is not a variant of the empirical mode decomposition method, but an alternative approach to the adaptive decomposition of functions.

FABEMD replaces scattered data interpolation for envelope estimation with application of maximum and minimum filters to the image, with the window size determined by the local extrema distances, and subsequent application of box filter to the resulting "rough" envelopes, and does this only 1 time instead of iterating until bidimensional IMF (BIMF) convergence in terms of standard deviation. To calculate the window size of the maximum, minimum and smoothing filters, minimum (or maximum) distances between local extrema are used, which produces so-called LD-OSFW (or HD-OSFW) variants of FABEMD.

It should also be noted that this method provides the ability to analyze images based on the study of the dependence of changes in the adaptively selected parameter of the method (window size): see, for example, (Guryanov and Krylov, 2017).

The algorithm of FABEMD is as follows:

1. Set the initial window size $w = 3$.
2. Find strict local maxima (minima) p in the window of size w: $\mathrm{I}(p) > \mathrm{I}(q)$ ($\mathrm{I}(p) < \mathrm{I}(q)$), $\forall q \in W_w(p)$, where $W_w(p)$ is a window of size w centered at p.
3. Determine the smallest distance between distinct local maxima (minima) d_{max} (d_{min}) and let $d = \min(d_{max}, d_{min})$ for LD-OSFW (or $d = \max(d_{max}, d_{min})$ for HD-OSFW).
4. Update the current window size
$$w := 2 \cdot \frac{d+1}{2} + 1.$$
5. Calculate upper and lower envelopes
$$\mathrm{U}(p) = \max_{q \in W_w(p)} \mathrm{I}(q),$$
$$\mathrm{L}(p) = \min_{q \in W_w(p)} \mathrm{I}(q).$$
6. Calculate the smoothed average
$$\mathrm{R}(p) = \frac{1}{w^2} \sum_{q \in W_w(p)} \frac{U(p) + L(p)}{2}.$$
7. Decompose I into the sum of $\mathrm{M} = \mathrm{I} - \mathrm{R}$ and R.
8. Iterate on R.

An example of the FABEMD result is presented in Fig. 2.

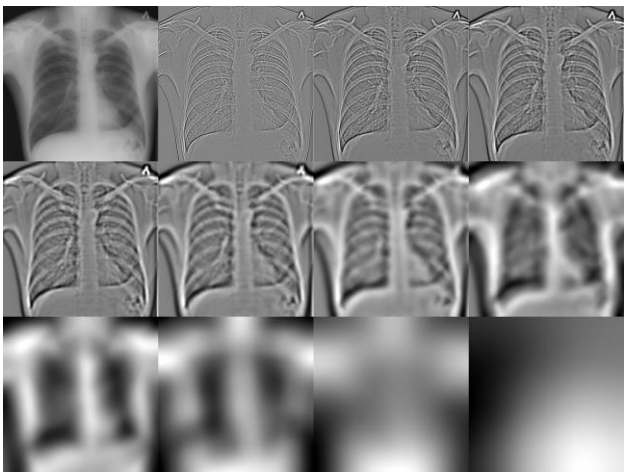

Figure 2. A chest X-ray and some of its BIMFs obtained by FABEMD in ascending order of the BIMF number

2.3 Applications

EMD and its variants are normally used to analyze and preprocess input data and are valued for being able to extract adaptive instance-wise nonlinear components with local certainty from the data. There are a number of applications in biomedical data processing (Yousefi Rizi, 2019). In chest X-ray analysis it is used as a contrast-enhancing method and can improve performance of deep-learning-based algorithms for diagnosis. For instance, in (Hasan, 2021) BEMD is used to remove the low frequency background from an input chest X-ray and emphasize the details before feeding the image into the network for COVID-19 diagnosis. In (Siracusano et al., 2023) FABEMD is utilized as the first step of a complex contrast enhancement pipeline, which

is meant to assist radiologists, but also can increase performance of deep-learning models.

They also find applications as a tool for data augmentation in some deep-learning-based algorithms. In (Nam et al., 2020) time series are augmented by exclusion of certain IMFs for an audio noise classification task. The augmentation was done IMF-wise, which increased the noise classification accuracy, but for general time series classification tasks showed suboptimal performance (Gao et al., 2023). In (Otero et al., 2022) two-dimensional curves of handwriting data are represented by two one-dimensional functions and each of these functions is recomposed by random sampling from its set of multivariate EMD (mEMD) IMFs. In (Yang et al., 2023) randomly sampled BIMFs of same-class images are fused by summation to increase the volume of training data. A similar approach is applied for graph MRI data augmentation in (Chen et al., 2022).

3. Method

Each k-th BIMF of a chest X-ray is assigned its own typical scale s_k equal to the distance between local extrema and the size of the envelope smoothing window w at the corresponding step of the FABEMD algorithm. It is assumed that BIMFs with large smoothing windows are unlikely to contain fine details crucial for diagnosis and can be removed. The result I_t, which is defined as

$$\mathrm{I}_t = \sum_{k:\,\frac{s_k}{\min(h,w)}<t} \mathrm{BIMF}_k,$$

where h and w are the height and the width of the X-ray, and t is the threshold value, is thought to be an image that is different from the original one, but still suitable for meaningful analysis (when t is reasonable). We add such background-removed X-rays to the training set. We used FABEMD with LD-OSFW to better capture local features, and made BIMF window size sequence to be non-decreasing by setting the local extrema search window size to the last envelope smoothing window size (therefore $\mathrm{s_k} \geq s_{k-1}, \forall k$) to ensure the BIMF fine and coarse details hierarchy and for faster convergence of the decomposition process. Examples of the resulting images are shown in Fig. 3.

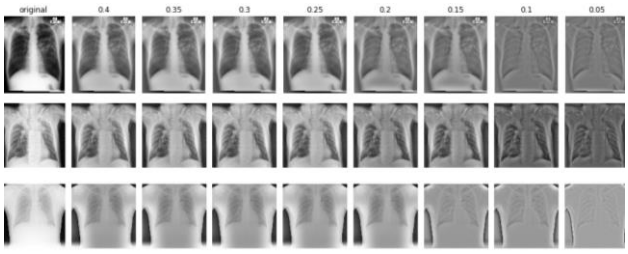

Figure 3. Examples of FABEMD-based background removal (the corresponding threshold value is written above each column)

4. Experimental Study Setup

4.1 Datasets

The following public datasets were considered:

- Montgomery (Candemir et al., 2013) and Shenzhen (Jaeger et al., 2013) were combined, since these datasets are used together in most works; the resolution is approx. 3000-4500 px by each side;
- DA and DB (Chauhan et al., 2014) were also combined due to their close relationship and small sizes; approx. 1000-3000 px by each side; some TB images in the DB dataset are missing;
- TBX11K (Liu et al., 2020); 512 px; only TB and healthy images were used;
- Sakha-TB (Pchelintsev et al., 2023) (8-bit version, approx. 1000x1000 px). This dataset was collected by the authors earlier in collaboration with a number of medical institutions of the Sakha Republic (Yakutia) region of Russia, and is believed to better represent the target data in this region.

The image counts are presented in Table 1. Each dataset was independently split into train (64%), validation (16%) and testing (20%) sets with class stratification.

Dataset	TB	Healthy	Total size
Montgomery	58	80	138
Shenzhen	336	326	662
DA	78	78	156
DB	47	75	122
TBX11K	800	3800	4600
Sakha-TB	400	400	800

Table 1. The number of images in the considered public datasets

4.2 Metrics and Evaluation

During the research we evaluated and analyzed the models' performance in terms of ROC AUC and Precision-Recall AUC (PR AUC). ROC AUC is a composite indicator for assessing classification algorithm quality based on sensitivity and specificity values widely used in medicine. Unlike such metrics as Precision, Recall, F1 or Accuracy, which evaluate the classification algorithm quality for a single fixed confidence threshold, ROC AUC measures the entire algorithm power. As for PR AUC, it is more indicative for imbalanced datasets, which is the case for TBX11K. However, during our experiments its behavior followed that of ROC AUC, so for some results we provide only ROC AUC for visual clarity.

All evaluations provided below were done on the test sets for all considered datasets by averaging of 3 independent training runs with different random seeds.

4.3 Models

4.3.1 Model Architecture and Training Procedure: For diagnosis we finetuned the ImageNet-pretrained EfficientNetV2-M with a 2-class classification head. The image preprocessing algorithm consisted of the following steps:

1. downsizing to the input size of 512x512 px;
2. center crop of 1% pixels from each side to remove frames present in some X-rays;
3. automatic image normalization:

$$h(x) = 255 \cdot \frac{x - p_{0.5}}{p_{99.5} - p_{0.5}},$$

where x is the pixel intensity of the input image, $p_{0.5}$ and $p_{99.5}$ are the 0.5%- and 99.5%-percentiles of the pixel intensities of the image;

4. automatic gamma correction:

$$g(x) = 255 \cdot \left(\frac{x}{255}\right)^{\gamma}, \qquad \gamma = \log_{\frac{\mu}{255}} 0.5,$$

where μ is the average intensity of the entire image;

5. an optional local contrast enhancement by CLAHE.

During training we augmented the data by random rotation, scaling and translation transformations, brightness and contrast adjustments, and used the cross-entropy loss, AdamW with LR of $5 \cdot 10^{-6}$, $\beta_1 = 0.9$, $\beta_2 = 0.999$, $\lambda = 0.01$, batch size of 32 and validation-loss-based ReduceLROnPlateau scheduler. The stopping criteria was based on the balanced accuracy score growth for the validation set, the final weights were chosen by the highest balanced accuracy score of the validation dataset.

The model without CLAHE preprocessing and the model with CLAHE processing step, both trained on the original data, are referred to as the "baseline model" and the "baseline CLAHE model" below. The CLAHE model was used to estimate the influence of the proposed data augmentation technique, when the base algorithm itself has a local contrast enhancement or normalization step.

4.3.2 CLAHE Preprocessing Parameters: The CLAHE algorithm has two parameters: window size, which determines the section of the image where histogram is equalized, and clip limit, which determines the contrast power. We defined the window size as an integer fraction of the size of the smaller side of the image. To choose the CLAHE parameters, a grid search was performed with the window size factor k grid of $\{4, 8\}$ and the clip limit l_c grid of $\{0.01, 0.005, 0.0025\}$. For each pair of parameters, a model was trained and its ROC AUC for each dataset was calculated. The results are presented in Fig. 4, all models were scored on the original test sets.

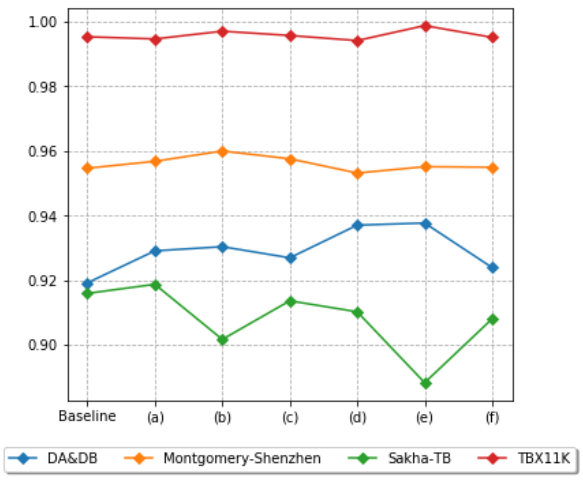

Figure 4. The dependence of the CLAHE model diagnosis performance on the CLAHE parameters:
(a) k=4, clip limit=0.01; (b) k=4, clip limit=0.005; (c) k=4, clip limit=0.0025; (d) k=8, clip limit=0.01; (e) k=8, clip limit=0.005; (f) k = 8, clip limit=0.0025.

We chose the parameters that allowed the model to perform as well as or better than the baseline model for every dataset: the window size factor of 4 and the clip limit equal to 0.01. Examples of the CLAHE impact on the data with such parameters can be seen in Fig. 5.

Figure 5. Examples of chest X-rays (above) and their CLAHE-processed versions (below)

4.4 Data Augmentation Procedure

Due to the computational complexity of FABEMD, before decomposition we downscaled all images larger than 1600x1600 px by integer factors to reach the resolution of approximately 1000x1000 px. After background removal we normalized the resulting images using 1%- and 99%-percentiles before saving. To isolate the influence of the downscaling operation, we compared the baseline model performance for the original and downscaled images (the results are shown in Table 2) and also tracked the performance changes during data augmentation for both the original and downscaled images.

Dataset	Original resolution	Downscaled
DA&DB	0.919	0.932
Montgomery-Shenzhen	0.955	0.958
Sakha-TB	0.916	0.916
TBX11K	0.995	0.995

Table 2. The baseline model performance (ROC AUC) for original and downscaled images

We chose a set of 8 background-removing thresholds ranging from 0.05 to 0.40: 0.05, 0.10, 0.15, 0.20, 0.25, 0.30, 0.35, 0.40, and added the corresponding augmented images from the training sets of all considered datasets to the global training set independently, obtaining 8 versions of joint original&augmented training datasets which in turn provided us 8 models. The finetuning procedure replicated that of the baseline models.

5. Results

5.1 Impact of Background Removal on Model Performance

We applied the baseline models to the FABEMD-augmented data and analyzed the models' performances in terms of ROC AUC and Precision-Recall AUC (PR AUC) as functions of the threshold for the considered threshold values. For each dataset and for each threshold value a set of test set images without the low-frequency background was created and then scored by the baseline model and the baseline CLAHE model. The results are presented in Fig. 6-7 and Fig. 8-9, respectively.

As the threshold value becomes lower, the datasets behave differently, but all of them fall below the initial level of performance at the threshold value of 0.20.

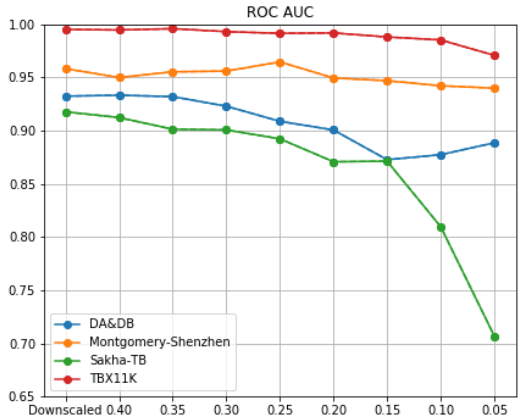

Figure 6. The dependence of the baseline model diagnosis performance (ROC AUC) on the X-ray background removal threshold value

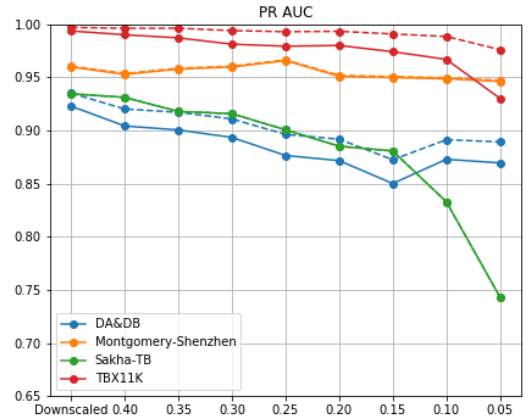

Figure 7. The dependence of the baseline model diagnosis performance (PR AUC) on the X-ray background removal threshold value

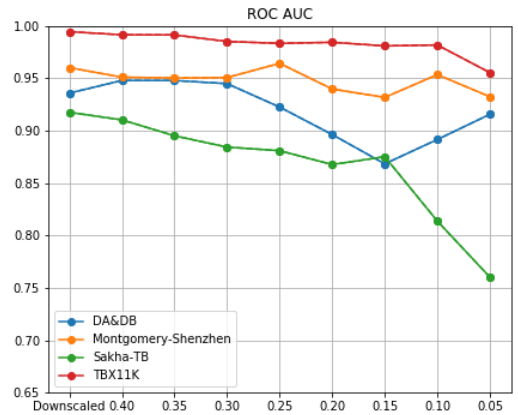

Figure 8. The dependence of the baseline CLAHE model diagnosis performance (ROC AUC) on the X-ray background removal threshold value

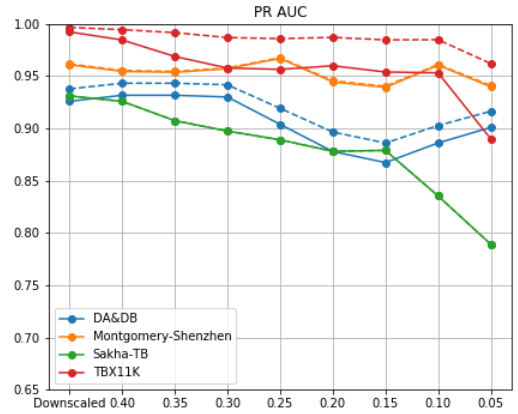

Figure 9. The dependence of the baseline CLAHE model diagnosis performance (PR AUC) on the X-ray background removal threshold value

The experiments showed an overall decline in performance with the growth of background-removal degree for all datasets for both baseline models, although the Montgomery-Shenzhen pair turned out to be the most resistant. The local contrast normalization preprocessing step indeed slightly reduced the performance drop for DA&DB and Sakha-TB datasets which suffered the most, but the previously rather stable dataset TBX11K took the hit instead.

5.2 Impact of FABEMD-based Data Augmentation on Model Performance

We measured the performance of all 8 models trained on the augmented data on the original and downscaled testing sets (without data augmentation). The results for models trained without CLAHE preprocessing step are shown in Fig. 10, and for models trained with CLAHE preprocessing are presented in Fig. 11.

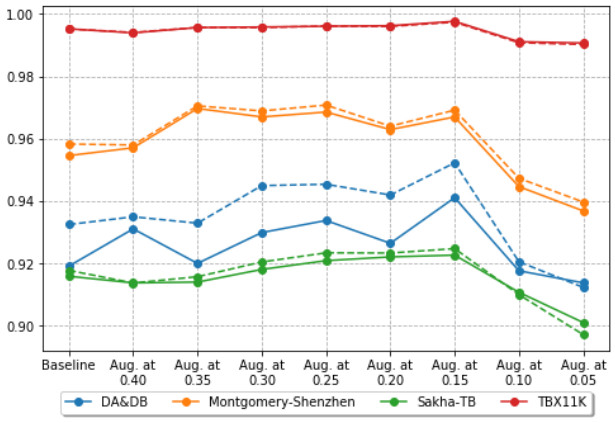

Figure 10. ROC AUC for non-CLAHE models trained on the original and augmented data with different thresholds. The solid lines indicate the original resolution data, the dashed lines show the downscaled data.

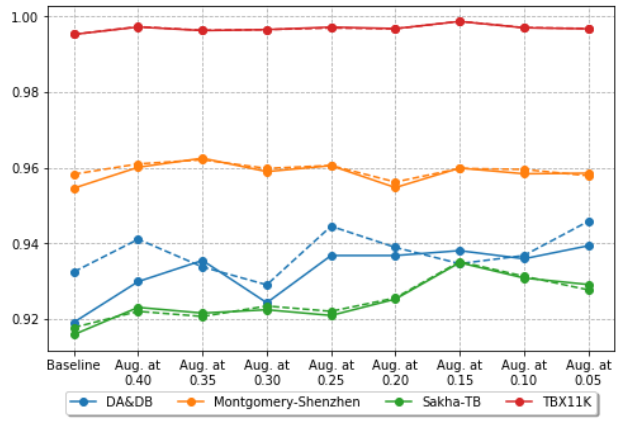

Figure 11. ROC AUC for CLAHE models trained on the original and augmented data with different thresholds. The solid lines indicate the original resolution data, the dashed lines show the downscaled data.

Both plots show positive impact on diagnosis performance, except for the case of the baseline non-CLAHE model and the most extreme background-removal threshold values. Notably the threshold value of 0.15 is the best option for every dataset and both model types overall.

It is noteworthy that CLAHE models not only stabilized the model quality response to data augmentation and prevented the performance drop after the threshold of 0.15, but also increased the positive effect of the proposed data augmentation method for DA&DB and Sakha-TB datasets. These datasets exhibited similar behavior in the diagnosis accuracy analysis during background-removal.

6. Conclusion

The proposed FABEMD-based image data augmentation method has shown its effectiveness for data augmentation for pulmonary tuberculosis diagnosis in chest X-rays. It also shows promise for use in various medical image analysis tasks. In future work optimization of this technique is going to be considered.

Acknowledgements (optional)

Work of Yakov Pchelintsev was supported by the Intellect Foundation.

References

Bhuiyan, S.M., Adhami, R.R., Khan, J.F., 2008a. Fast and adaptive bidimensional empirical mode decomposition using order-statistics filter based envelope estimation. *EURASIP Journal on Advances in Signal Processing*, 2008, 1–18.

Bhuiyan, S.M., Adhami, R.R., Khan, J.F., 2008b. A novel approach of fast and adaptive bidimensional empirical mode decomposition. *2008 IEEE International Conference on Acoustics, Speech and Signal Processing*, IEEE, 1313–1316.

Candemir, S., Jaeger, S., Palaniappan, K., Musco, J.P., Singh, R.K., Xue, Z., Karargyris, A., Antani, S., Thoma, G., McDonald, C.J., 2013. Lung segmentation in chest radiographs using anatomical atlases with nonrigid registration. *IEEE transactions on medical imaging*, 33(2), 577–590.

Chauhan, A., Chauhan, D., Rout, C., 2014. Role of Gist and PHOG features in computer-aided diagnosis of tuberculosis without segmentation. *PloS one*, 9(11), e112980.

Chen, X., Li, B., Jia, H., Feng, F., Duan, F., Sun, Z., Caiafa, C.F., Sol´e-Casals, J., 2022. Graph Empirical Mode Decomposition-Based Data Augmentation Applied to Gifted Children MRI Analysis. *Frontiers in Neuroscience*, Volume 16.

Gao, Z., Liu, H., Li, L., 2023. Data Augmentation for Time-Series Classification: An Extensive Empirical Study and Comprehensive Survey. *arXiv e-prints*, arXiv:2310.10060.

Guryanov, F., Krylov, A., 2017. Fast medical image registration using bidirectional empirical mode decomposition. *Signal Processing: Image Communication*, 59, 12-17.

Hasan, N.I., 2021. A Hybrid Method of COVID-19 Patient Detection from Modified CT-Scan/Chest-X-Ray Images Combining Deep Convolutional Neural Network And Two-Dimensional Empirical Mode Decomposition. *Computer Methods and Programs in Biomedicine Update*, 1, 100022.

Huang, N.E., Shen, Z., Long, S.R., Wu, M.C., Shih, H.H., Zheng, Q., Yen, N.-C., Tung, C.C., Liu, H.H., 1998. The empirical mode decomposition and the Hilbert spectrum for nonlinear and non-stationary time series analysis. *Proceedings of the Royal Society of London. Series A: Mathematical, Physical and Engineering Sciences*, 454(1971), 903-995.

Jaeger, S., Karargyris, A., Candemir, S., Folio, L., Siegelman, J., Callaghan, F., Xue, Z., Palaniappan, K., Singh, R.K., Antani, S., Thoma, G., Wang, Y.-X., Lu, P.-X., McDonald, C.J., 2013. Automatic tuberculosis screening using chest radiographs. *IEEE transactions on medical imaging*, 33(2), 233–245.

Liu, Y.,Wu, Y.-H., Ban, Y.,Wang, H., Cheng, M.-M., 2020. Rethinking computer-aided tuberculosis diagnosis. *Proceedings of the IEEE/CVF conference on computer vision and pattern recognition*, 2646–2655.

Nam, G.-H., Bu, S.-J., Park, N.-M., Seo, J.-Y., Jo, H.-C., Jeong, W.-T., 2020. Data augmentation using empirical mode decomposition on neural networks to classify impact noise in vehicle. *ICASSP 2020 - 2020 IEEE International Conference on Acoustics, Speech and Signal Processing (ICASSP)*, 731–735.

Nia, S.N., Shih, F.Y., 2024. Medical X-Ray Image Enhancement Using Global Contrast-Limited Adaptive Histogram Equalization. *International Journal of Pattern Recognition and Artificial Intelligence*, 38(12), 2457010.

Nunes, J., Bouaoune, Y., Delechelle, E., Niang, O., Bunel, P., 2003. Image analysis by bidimensional empirical mode decomposition. *Image and Vision Computing*, 21(12), 1019-1026.

Oloko-Oba, M., Viriri, S., 2022. A systematic review of deep learning techniques for tuberculosis detection from chest radiograph. *Frontiers in Medicine*, 9, 830515.

Otero, J.F. A., López-de-Ipina, K., Caballer, O.S., Marti-Puig, P., Sánchez-Méndez, J.I., Iradi, J., Bergareche, A., Solé-Casals, J., 2022. EMD-based data augmentation method applied to handwriting data for the diagnosis of Essential Tremor using LSTM networks. *Scientific Reports*, 12(1), 12819.

Pchelintsev, Y., Khvostikov, A., Buchatskaia, O., Nikiforova, N., Shepeleva, L., Prokopev, E., Parolina, L., Krylov, A., 2023. Robustness analysis of chest X-ray computer tuberculosis diagnosis. *Computational Mathematics and Modeling*, 33(4), 472–486.

Pizer, S.M., Amburn, E.P., Austin, J.D., Cromartie, R., Geselowitz, A., Greer, T., ter Haar Romeny, B., Zimmerman, J.B., Zuiderveld, K., 1987. Adaptive histogram equalization and its variations. *Computer vision, graphics, and image processing*, 39(3), 355–368.

Pooch, E.H., Ballester, P., Barros, R.C., 2020. Can we trust deep learning based diagnosis? The impact of domain shift in chest radiograph classification. *Thoracic Image Analysis: Second International Workshop, TIA 2020*, Springer International Publishing, 74–83.

Rahman, T., Khandakar, A., Qiblawey, Y., Tahir, A., Kiranyaz, S., Abul Kashem, S.B., Islam, M.T., Al Maadeed, S., Zughaier, S.M., Khan, M.S., Chowdhury, M.E., 2021. Exploring the effect of image enhancement techniques on COVID-19 detection using chest X-ray images. *Computers in Biology and Medicine*, 132, 104319.

Rui, W., Guoyu, W., 2017. Medical X-ray image enhancement method based on TV-homomorphic filter. *2017 2nd International Conference on Image, Vision and Computing (ICIVC)*, 315–318.

Santosh, K., Allu, S., Rajaraman, S., Antani, S., 2022. Advances in deep learning for tuberculosis screening using chest X-rays: the last 5 years review. *Journal of Medical Systems*, 46(11), 82.

Setty, S., Srinath, N.K., Hanumantharaju, M.C., 2013. Development of multiscale retinex algorithm for medical image enhancement based on multi-rate sampling. *2013 International Conference on Signal Processing, Image Processing & Pattern Recognition*, 145–150.

Singh, M., Pujar, G.V., Kumar, S.A., Bhagyalalitha, M., Akshatha, H.S., Abuhaija, B., Alsoud, A.R., Abualigah, L., Beeraka, N.M., Gandomi, A.H., 2022. Evolution of machine learning in tuberculosis diagnosis: a review of deep learning-based medical applications. *Electronics*, 11(17), 2634.

Siracusano, G., La Corte, A., Nucera, A.G., Gaeta, M., Chiappini, M., Finocchio, G., 2023. Effective processing pipeline PACE 2.0 for enhancing chest X-ray contrast and diagnostic interpretability. *Scientific Reports*, 13(1), 22471.

Sweeney-Reed, C.M., Nasuto, S.J., Vieira, M.F., Andrade, A.O., 2018. Empirical Mode Decomposition and its Extensions Applied to EEG Analysis: A Review. *Advances in Data Science and Adaptive Analysis*, 10(02), 1840001.

Victor, 2012. Introduction to the empirical mode decomposition method. MQL5. https://www.mql5.com/en/articles/439 (18 July 2012). [Online; accessed 30-April-2025].

World Health Organization, 2024. *Global tuberculosis report 2024*. World Health Organization.

Xue, Z., Yang, F., Rajaraman, S., Zamzmi, G., Antani, S., 2023. Cross dataset analysis of domain shift in CXR lung region detection. *Diagnostics*, 13(6), 1068.

Yang, D., Zhang, B., Wang, Y., Hu, B., Huang, J., 2023. BIMFM: A bidimensional intrinsic mode functions mixup strategy for thermal imagery data augmentation. *2023 IEEE 6th Information Technology, Networking, Electronic and Automation Control Conference (ITNEC)*, 6, IEEE, 1719–1724.

Yousefi Rizi, F., 2019. A Review of Notable Studies on Using Empirical Mode Decomposition for Biomedical Signal and Image Processing. *Signal Processing and Renewable Energy (SPRE)*, 3(4), 89–113.

Zeyu, D., Yaakob, R., Azman, A., 2022. A review of deep learning-based detection methods for tuberculosis. *2022 IEEE International Conference on Computing (ICOCO)*, IEEE, 68–73.

Zhao, Z., Zhou, Y., 2016. PLIP based unsharp masking for medical image enhancement. *2016 IEEE International Conference on Acoustics, Speech and Signal Processing (ICASSP)*, 1238–1242.